Chapter 2 – RARE-EARTH-DOPED FIBERS: BACKGROUND

2.1 INTRODUCTION

Fiber lasers are efficient, powerful and versatile waveguide resonant devices that comprise glass optical fiber waveguides for optical gain and Fabry-Pérot resonators for optical feedback. Rapid developments in fabrication capabilities now allow fibers composed of ultralow-loss silicate glass with low scattering, impurity losses and material imperfections, thus providing enormous flexibility in the characteristics and quantity of light that can be generated from fiber lasers. Passively air-cooling an optical fiber is simple owing to its large surface-area-to-volume ratio. Optical excitation using multi-mode semiconductor diode lasers is straightforward and efficient with cladding pumping [1], particularly when the axial symmetry of the fiber is broken [2], and efficiently excites the single-mode core of the fiber to create near-diffraction-limited output with significant enhancement in the brightness [3]. Although doping silicate glass optical fibers using rare-earth cations introduces additional Rayleigh scattering, this drawback is small compared with the gain enhancement. Furthermore, diluted (< 0.1 mol %) rare-earth cation concentrations have a background loss [4] of less than 2 dB km^{-1}, a value that is commensurate with conventional fiber. The lack of long-range order in a silicate glass means that the bandwidth for pump absorption and gain can be up to 50 THz, which relaxes the wavelength tolerance for excitation and creates opportunities for broad tuning and ultrashort pulse generation. The small dimensions of the modes propagating in the core of the fiber provide low-threshold and high-gain characteristics with near-maximum efficiency.

2.2 FIBER LASERS OPERATING AT 1 μM

The highest values of output power and efficiency have been achieved at around 1 μm using Yb^{3+} cations doped into the core of silicate glass fiber and commercial systems [5] capable of supplying output powers of up to 50 kW are now used for a variety of applications, including cutting and welding in the automotive industry. There are a number of reasons for this success. First, the quantum efficiency of the laser transition is close to 100% while the quantum defect, that is, the difference between the pump and laser photon energies, is typically less than 10%. Second, the use of silicate glass optical fiber provides the system with a significant degree of robustness and power-handling capability. Yb^{3+}-doped silicate glass fiber lasers emitting at around 1 μm are therefore incredibly practical devices.

2.3 FIBER LASERS OPERATING BEYOND 1 μM

2.3.1 Pros and Cons

Extending the emission wavelength into the mid-infrared is necessary for a large number of existing and future applications, including IRCM and spectroscopy [6]. The task of engineering a fiber laser becomes easier at longer wavelengths, owing to a number of optical scaling factors. The mode area of the lowest-order mode scales as λ^2, where λ is the laser wavelength; for example, the mode at 2 μm has four times the area of the same mode at 1 μm. This has a profoundly beneficial effect on the power scaling potential of fiber lasers. Because losses due to non-linearity scale with light intensity, Brillouin and Raman scattering are lower at longer wavelengths and so optical damage thresholds are increased. The size of the mode can also be increased by using smaller refractive index contrasts [7] or holey fiber [8]. Translating these methods to longer wavelengths provides further potential for power scaling.

Moving further into the infrared and away from the bandgap of a given glass means that more photons are required to bridge the bandgap, which raises the ablative threshold and thus lowers the loss from two-photon absorption. Stokes emission generated from Raman scattering is also weaker at longer wavelengths [9]. The formation of color centers resulting from localized charge regions is a problem for some Yb^{3+}-doped

silicate glasses because the resulting absorption features located in the visible region have long absorption tails that overlap with the pump and emission wavelengths of Yb^{3+} [10],[11]. The absorption strength diminishes and therefore potentially becomes less problematic at longer wavelengths; for example, with silicate glass fiber lasers that operate at 2 µm.

Unfortunately, extending the emission wavelength of fiber lasers beyond the natural loss-minimum of silicates at 1.5 µm remains a significant challenge. The physical properties of the glass comprising some fibers, such as high background absorption, poor thermal conductivity and low glass transition temperature, negatively impact the output performance beyond this loss minimum. Infrared transmission in the glass is controlled by the phonon density of states, which means that the longest emitting wavelength from a fiber laser is always shorter than its maximum transmissible wavelength because the phonon density of states determines the radiative efficiencies of the fluorescence transitions of the rare-earth cations. Significant research has been directed towards the development of glasses that have the combined characteristics of low maximum phonon energy and fiber 'drawability' while maintaining amorphousness and low loss. Only a small number of glasses currently have these characteristics.

2.3.2 Laser Transitions of the Rare-Earth Cations

The lasing wavelength of fiber lasers is determined by the fluorescence transitions of the rare-earth cation doped into the core of the fiber. Figure 2-1 shows the laser transitions responsible for infrared emission from several rare-earth cation-doped fiber lasers. With a few exceptions, rare-earth cations are consistently in the trivalent oxidation state, and the associated electronic transitions of the cations are the foundation of infrared fiber lasers.

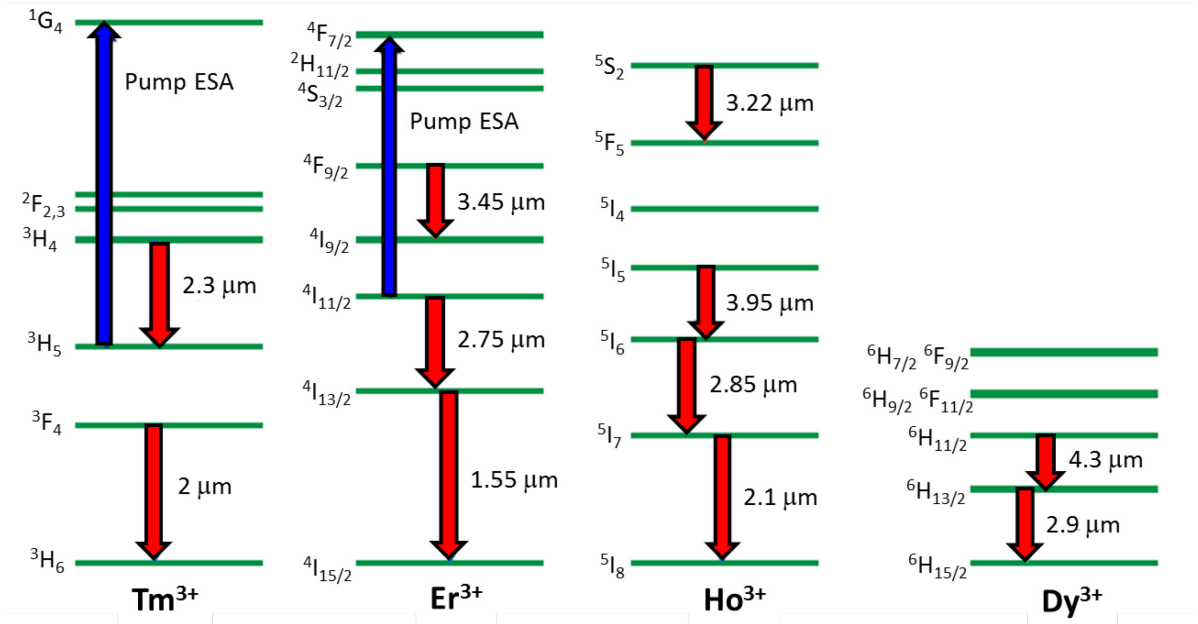

Figure 2-1: Laser Transitions of Rare-Earth Cations for Emission Wavelengths Longer than 1.5 µm.

Phonon broadening acts similarly on all of the rare-earth cations and is therefore homogeneous, but the perturbations to the energy levels of the cations by the surrounding electric fields from nearby glass atoms vary from one cation site to another, which makes them inhomogeneous and temperature-independent. In covalently bonded glasses such as silica, the rare-earth cations form inter-network regions [12] (percolation

channels) comprised of rare-earth cations that bond ionically to non-bridging oxygen atoms that interface with the main covalently bonded network regions. Because their large cationic field strength (defined as Z/r^2, where Z is the atomic number and r is the radius of the ion) requires a high coordination number, rare-earth cations tend to cluster in the inter-network regions to share non-bridging oxygen atoms. The nephelauxetic causes the absorption and emission peaks of rare-earth cation transitions to red-shift to longer wavelengths with increasing covalency of the bonding between the network formers [13].

The relevant fluorescence spectra of the infrared transitions from fiber lasers are shown in Figure 2-2 [14]. The quasi-three-level transitions of the large-Z rare-earth cations Tm^{3+}, Ho^{3+} and Er^{3+}, which fluoresce in the range of 1.5 – 2.2 µm, are responsible for the highest powers available from fiber lasers emitting in the $\lambda > 1.5$ µm region of the near-infrared. The output power performance of such devices relates to strong absorption by cations, which overlaps with the emission from commercial off-the-shelf high-power diode lasers and the excellent physical properties of the silicate glasses used to create the fiber. Extending the laser wavelength further into the infrared has necessitated the use of fluoride glass fiber, owing to its low phonon energy. For the fluorides, the fluorescence spectra tend to cluster in a region that spans approximately 0.6 µm.

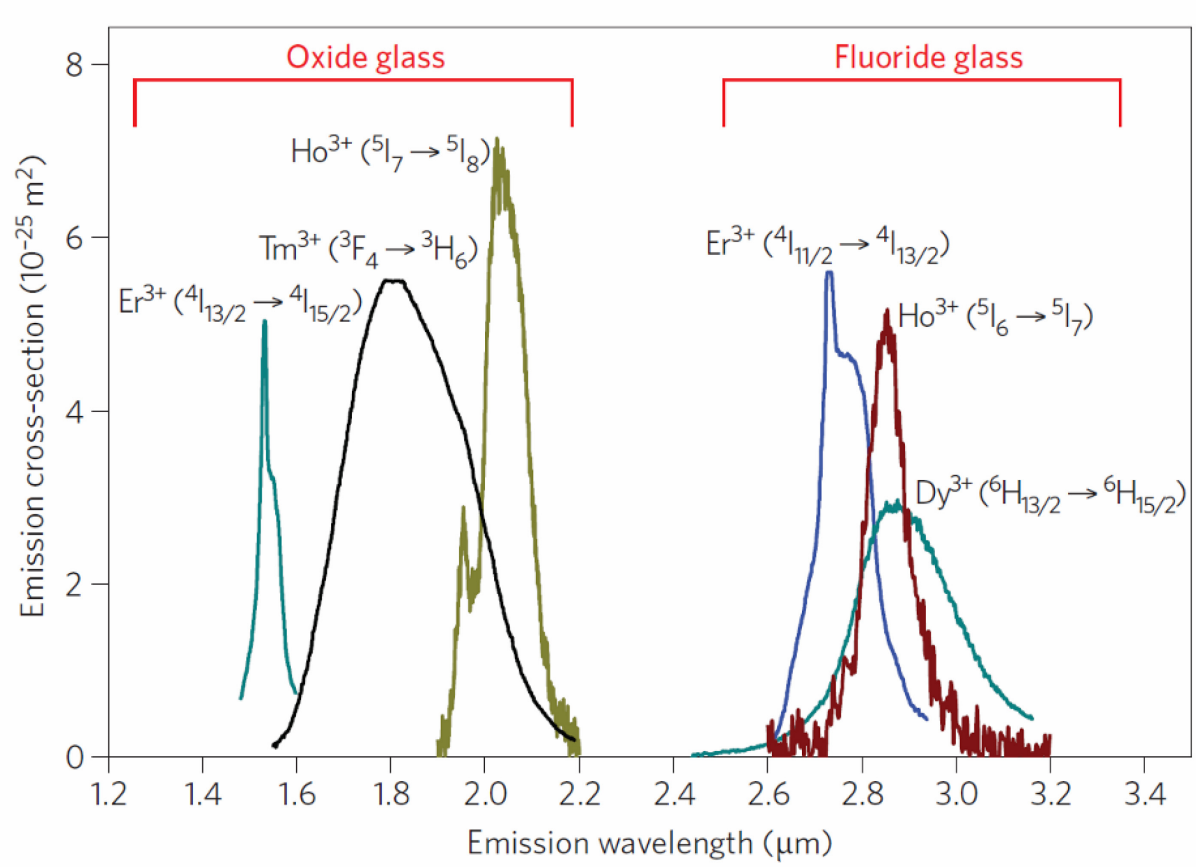

Figure 2-2: Fluorescence Spectra of the Rare-Earth Cation Laser Transitions Used in Fiber Lasers Emitting at Wavelengths Greater Than 1.5 µm. (Oxide glass is a silicate and fluoride glass is ZBLAN) (after S. Jackson [14]).

2.3.3 Host Materials

The typically long (> 1 m) optical path length of a fiber laser means that glasses must exhibit low impurity, low scattering loss, a large Hruby parameter [49] (glass stability) and a low maximum phonon energy.

For emission in the 1 – 2.2 μm region, the low loss and physical strength of silicate glasses has made them remarkably useful hosts for rare-earth cations emitting in this region. Fluoride glasses have high efficiency and moderate output power in the 2.3 – 3.5 μm region. Beyond 3.5 μm, however, only a small number of glasses have the suitably low phonon energy that provides the necessarily high transmission of the fiber and sufficient radiative efficiency for the rare-earth cation transitions.

2.3.3.1 Silicates

Silicate glasses remain the most successful fiber host materials. A high laser damage threshold [50] of approximately 500 MW/cm^2 for doped silicate glass ensures robust high-power operation, and fabrication using modified chemical vapor deposition ensures excellent glass purity. Silicate glasses have high melting points, relatively low thermal expansion coefficients, large tensile strengths, low refractive indices and low non-linearities. All glasses have a low second-order non-linearity, although loss to third-order non-linear processes such as stimulated Raman scattering can be substantial because of the long fiber length and large light intensity in the active core. Silicate glasses consist of strongly covalently bonded atoms that form a disordered matrix with a range of bond lengths and angles. Silica can sustain maximum phonon energies [51] of up to 1,100 cm^{-1}, which sets an upper limit on the emission wavelength. The giant covalent structure of silicate glasses leads to excellent mechanical properties. The maximum 'lattice' vibration or 'phonon' energy is the most active in multi-phonon decay, and the fluctuating Stark field surrounding the rare-earth cation arising from the vibration of the surrounding anions and cations induces non-radiative decay. Because the bandgap of silica is 9 eV, loss to two-photon absorption is small at infrared wavelengths and Rayleigh scattering loss [52] from the frozen-in density fluctuations in the glass can be as low as 0.15 dB km^{-1}. When network formers such as Al_2O_3 and P_2O_5 are added to silica [53], they create the solvation shells necessary for improved rare-earth cation solubility to counteract clustering. Unfortunately, Rayleigh scattering loss increases as a result of the extra refractive index inhomogeneities introduced by the addition of these dopants. Emission at 2 μm from Tm^{3+} and Ho^{3+} cations doped into silicate glasses is highly developed, and a number of commercial systems are now available. The longest laser wavelength [54] from a silicate glass fiber laser is currently 2.188 μm; lasing at longer wavelengths is not expected to be possible in the majority of silicate glasses due to significant phonon quenching.

2.3.3.2 Fluorides

One of the most successful compositions among fluoride glasses is ZBLAN [55], which is comprised of 53 mol % ZrF_4, 20 mol % BaF_2, 4 mol % LaF_3, 3 mol % AlF_3 and 20 mol % NaF. The ZBLAN composition can be varied to introduce certain characteristics: for example, adding PbF_2, ZnF_2 or CaF_2 modifies the viscosity and refractive index; substituting a proportion of ZrF_4 for ThF_4 creates better stability against crystallization; and substituting ZrF_4 with HfF_4 lowers the refractive index. Fluoride fiber preforms can be created by a number of casting processes [56],[57], although crystallization during cooling and reheating often creates scattering centers that limit the dimensions of the preform and the maximum length of useful fiber. Geometrical defects such as inclusions and bubbles formed during fabrication also cause scattering. Reducing the casting pressure of ZBLAN eliminates bubble formation to allow, when combined with anhydrous fluoride precursors, a minimum fiber loss of 0.65 dB km^{-1} at 2.59 μm and < 20 dB km^{-1} at 2.9 μm, which is where the O–H impurity stretching vibration in ZBLAN is located [58].

The maximum phonon energy of ZBLAN [59] is approximately 565 cm^{-1}, which allows fluorescence at room temperature to occur from rare-earth cation transitions comprised of energy gaps larger than 2,825 cm^{-1} (that is, $\lambda <$ 3.5 μm). ZBLAN has low optical dispersion, a low refractive index of 1.49 and a broad transmission window (defined here to have an attenuation of less than 200 dB km^{-1}) in the range of 0.2 – 4.5 μm [60]. Compared with silicate glasses, the lower maximum phonon energy of ZBLAN (and thus the extended infrared transmission) relates to the weaker bond strength and larger reduced mass of the atoms comprising the glass. The fluoride anion is singly charged, which, when combined with weaker bonding, means a higher chemical reactivity compared with silicates, although rare-earth cations substitute the

La3+ cations of the glass to provide comparatively higher doping levels without clustering. The optical damage threshold [61] of ZBLAN for 10 ms pulses at 2.8 μm is approximately 25 MW cm^{-2}, which restricts the achievable peak power levels compared with silicates. However, because the Raman gain coefficient is comparatively smaller [62], significant loss to Raman scattering may never be a concern in future high-power infrared fiber lasers using this glass. The higher thermal loading resulting from the moderate efficiency of 3-μm-class fiber lasers (for which ZBLAN fibers are used), combined with the comparatively poorer physical properties of fluoride glasses, has made power-scaling a significant challenge. The maximum output power from ZBLAN-based fiber lasers is currently 24 W at 2.7 μm [21] and 20 W at 1.94 μm [16].

2.3.3.3 Alternatives

There is ongoing development in the fabrication and testing of glasses for achieving longer emission wavelengths. Germanate glasses [63] have robust mechanical qualities, maximum phonon energies [64] of 900 cm^{-1} and large rare-earth cation solubilities, which allow cluster-reduced Tm^{3+} concentrations in fibers for high-efficiency 1.9 μm emission [65] and short-length devices providing narrow-linewidth output [66]. However, the practicality of germanate glasses for emission beyond 2 μm is reliant on effective removal of OH^- impurity from the glass, which is difficult to achieve. Tellurite glass fiber [67] is a promising alternative, but, like most oxide glasses fabricated from solid-state precursor materials, it contains relatively high concentration of OH^-. Energy transfer from excited Er^{3+} cations to OH^- impurities, combined with the low radiative efficiency of the upper laser level, is sufficient to suppress 3 μm lasing in state-of-the-art Er^{3+}-doped tellurite glass [68]. Chalcogenides [69], glasses based on chalcogens S, Se or Te, are a widely investigated group whose high refractive indices result in large absorption and emission cross-sections. Maximum phonon energies depend on the exact composition of the glass, with values of 350 – 425 cm^{-1} for sulphide glasses [70], 250 – 300 cm^{-1} for selenide glasses [71] and 150 – 200 cm^{-1} for telluride glasses [72]. Optical transmission reaches well into the mid-infrared, up to 15 μm in the case of telluride glass [73], and fluorescence has been measured in sulphide, selenide and telluride glasses from a number of rare-earth cation transitions with emission wavelengths as long as 8 μm [74]. The only demonstration of a rare-earth-doped chalcogenide fiber laser was based on Nd^{3+} emitting at 1.08 μm [75], in which the addition of La_2O_3 to gallium chalcogen glass in order to avoid crystallization during fiber drawing [76] most likely created energetic phonons that suppressed longer-wavelength emission [77]. No laser emission beyond 1 μm has yet been achieved using a rare-earth cation-doped chalcogenide glass fiber, presumably due to the crystallization tendency upon rare-earth doping. Ge–Sb and Ge–As chalcogen glasses, for example, are strongly covalently bonded, which makes the incorporation of rare-earth cations a significant challenge. Alternative co-dopants for chalcogen-based glasses are being developed to improve rare-earth cation solubility and eliminate crystallization [78].

2.3.4 State-of-the-Art CW Fiber Lasers

Despite the variety of rare-earth cation transitions and host materials that have been tested for fiber laser emission, the maximum CW output power produced from demonstrated fiber lasers has a clear exponential decrease when plotted as a function of emission wavelength (Figure 2-3). Table 2-1 lists the maximum output power from reported fiber lasers [14]-[27].

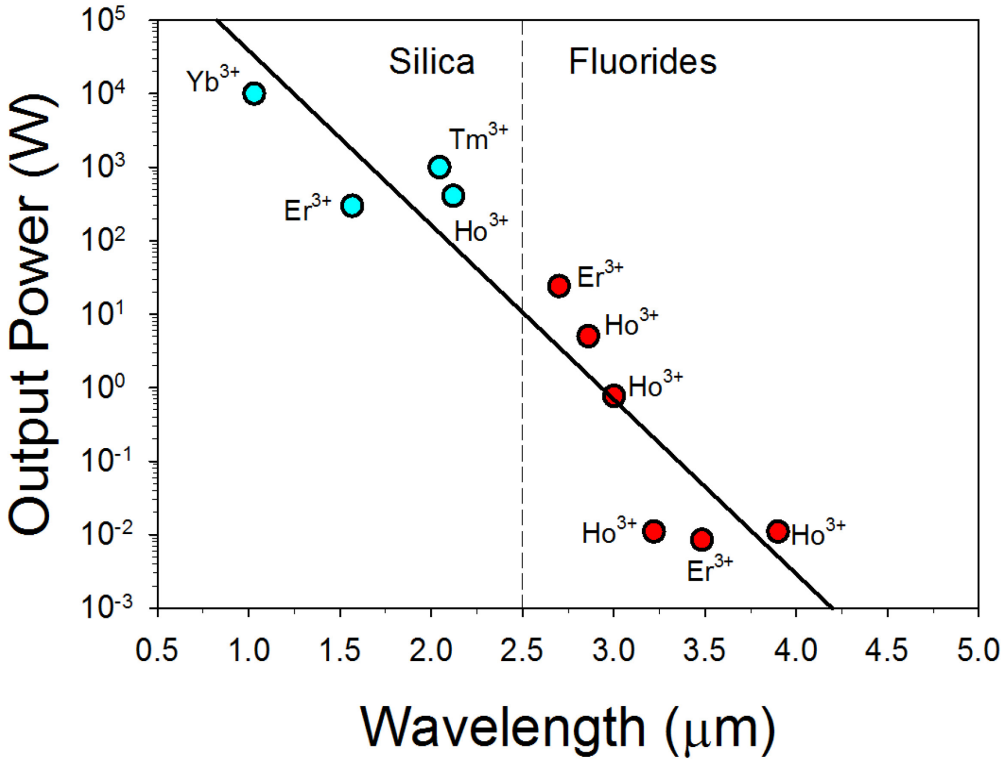

Figure 2-3: Output Power at Different Laser Wavelengths Using Rare-Earth-Doped Silica (Blue Circles) and ZBLAN (Red Circles) Fibers, Respectively. The dashed line is a guide to the eye.

Table 2-1: Characteristics of Infrared Fiber Lasers with Emission Wavelengths ≥ 1.5 μm.

Dopant(s)	Host Glass	Pump λ (μm)	Laser λ (μm)	Transition	Output Power (W)	% Slope Efficiency	Reference
Er^{3+}, Yb^{3+}	Silicate	0.975	1.5	$^4I_{13/2} \rightarrow {}^4I_{15/2}$	297	19	15
Tm^{3+}, Ho^{3+}	ZBLAN	0.792	1.94	$^3F_4 \rightarrow {}^3H_6$	20	49	16
Tm^{3+}	Silicate	0.793	2.05	$^3F_4 \rightarrow {}^3H_6$	1,050	53	17
STm^{3+}, Ho^{3+}	Silicate	0.793	2.1	$^5I_7 \rightarrow {}^5I_8$	83	42	18
Ho^{3+}	Silicate	1.950	2.12	$^5I_7 \rightarrow {}^5I_8$	407	~ 30	19
Tm^{3+}	ZBLAN	1.064	2.31	$^3H_4 \rightarrow {}^3H_5$	0.15	8	20
Er^{3+}	ZBLAN	0.975	2.8	$^4I_{11/2} \rightarrow {}^4I_{13/2}$	24	13	21
Ho^{3+}, Pr^{3+}	ZBLAN	1.1	2.86	$^5I_6 \rightarrow {}^5I_7$	2.5	29	22
Dy^{3+}	ZBLAN	1.1	2.9	$^6H_{13/2} \rightarrow {}^6H_{15/2}$	0.275	4.5	23
Ho^{3+}	ZBLAN	1.15	3.002	$^5I_6 \rightarrow {}^5I_7$	0.77	12.4	24
Ho^{3+}	ZBLAN	0.532	3.22	$^5S_2 \rightarrow {}^5F_5$	0.011	2.8	25
Er^{3+}	ZBLAN	0.653	3.45	$^4F_{9/2} \rightarrow {}^4I_{9/2}$	0.008	3	26
Ho^{3+}	ZBLAN	0.89	3.95	$^5I_5 \rightarrow {}^5I_6$	0.011	3.7	27

The primary cause of this power drop is the increase in quantum defect at longer wavelengths. Efficient high-power diode lasers, the traditional pump sources for silicate glass fiber lasers, typically emit light in the near-infrared region close to 1 μm. Although it would be ideal to use these efficient pump sources for all fiber lasers, the larger quantum defect at longer wavelengths creates heat that becomes an ever-increasing fraction of the absorbed pump energy. The small active-core volume of an optical fiber relative to the total fiber volume of a double-clad fiber results in a small temperature gradient [28]. The temperature within the fiber is governed strongly by the degree of cooling at the air–fiber boundary, which is improved by a large surface area (that is, a larger pump-core diameter). The excellent cooling properties of optical fibers therefore help to alleviate the problem of the growing quantum defect. Developing efficient longer-wavelength pump sources and selecting more appropriate laser transitions can effectively reduce the quantum defect and improve output performance. Laser transition cascading [29], in which multiple transitions lase simultaneously after a single pump photon excitation, offers the opportunity for better photon-to-photon conversion efficiencies and is particularly suited to longer-wavelength transitions for reducing heat loads and improving power-scaling opportunities.

Fiber lasers employing the Tm^{3+} cation [30]-[33] with emission at around 2 μm are the most powerful, efficient and developed of these fiber lasers. These devices are excited with established diode lasers [34] emitting at 0.79 μm, and their output can be tuned from at least 1.86 μm to around 2.09 μm. With the implementation of Tm^{3+} concentrations exceeding 2.5 wt %, combined with cluster-reducing co-dopants that mitigate gain-lowering energy transfer up-conversion processes, cross-relaxation between neighboring Tm^{3+} cations can nearly double the slope efficiency [35]. Cross-relaxation ('two-for-one' excitation) is resonant in silicate glass, thus providing one of the most efficient ways to generate 2 μm light from commercial diode laser pump sources.

The $^5I_7 \rightarrow {}^5I_8$ transition of Ho^{3+} has a peak emission wavelength of 2.1 μm, which overlaps with an important atmospheric transmission window. This transition is also acceptable for resonant pumping with Tm^{3+}-doped silicate glass fiber lasers [36], which introduces a small quantum defect of < 7%. Ho^{3+} fiber lasers were initially co-doped with Tm^{3+} sensitizer cations to exploit the diode-pumpable absorption of Tm^{3+} [37], although loss of excitation to energy-transfer up-conversion and reversible energy-transfer between the first excited states of Tm^{3+} and Ho^{3+} limited the power, extractable energy and efficiency of this technique. Doping silicate glass with only Ho^{3+} cations supports a large short-pulse extraction efficiency and has the potential to reduce the sensitivity of gain to temperature. The demonstration of direct diode pumping with Ho^{3+} [38] opens up additional power-scaling opportunities.

The fluoride glass fiber has a lower phonon energy than silica and so enables emission at longer wavelengths. Er^{3+}-doped fluoride fiber laser can be tuned across the range of 2.71 – 2.88 μm [39]. Engineering the stability and efficiency of the output from a fluoride fiber laser, a necessary requirement for commercial exploitation, is made possible by writing Bragg gratings [40] and splicing glass caps [41] to the ends of the fiber. The overlap of the upper laser level absorption with highly developed diode lasers emitting at 0.98 μm, combined with effective cooling of Er^{3+}-doped double-clad fluoride fiber, has resulted in output powers of up to 24 W at wavelengths of around 2.8 μm [21]. When high-quality Er^{3+}-doped double-clad fluoride fiber with a background loss of < 100 dB km^{-1} is combined with a high Er^{3+} concentration and an optimally engineered fiber laser resonator, energy transfer up-conversion (Figure 2-1) effectively de-populates the lower laser level and 'recycles' the excitation to produce slope efficiencies of 35.6% [42]. Engineering the effective de-population of the lower laser level is required because the upper laser level has a shorter luminescence lifetime than the lower laser level [43]. Cascade lasing [44]-[46] the transitions of 2.8 μm and 1.5 μm offers a solution to the problem of managing the heat generated due to the comparatively low optical conversion efficiencies of single-transition Er^{3+} systems. Pump-excited state absorption from the upper laser level (Figure 2-1) creates a roll-off in the calculated [47] and measured [42] output power and thus presents a significant problem for power-scaling the output from Er^{3+}-doped fluoride fiber lasers pumped to the upper laser level.

Ho^{3+}-doped fluoride fiber [48], which has a wide emission range of 2.8 – 3.02 μm for the $^5I_6 \rightarrow {}^5I_7$ transition, has the advantage of reduced pump-excited state absorption and a higher Stokes limit when the upper laser level is diode-pumped at 1.15 μm. However, the present maximum output power of this system is an order of magnitude lower than that of an Er^{3+}-doped fluoride fiber laser because the low demand for diode lasers operating at 1.15 μm means that beam-combining and brightness-conserving power-scaling technologies have not been expanded to these pump sources. An opportunity to increase the power and wavelength of 3 μm-class fiber lasers has recently been demonstrated [24] using cascade lasing of both the 2.9 μm and 2.1 μm transitions of Ho^{3+}. Laser emission at 3.9 μm was demonstrated under cryogenic conditions from a Ho^{3+}-doped fluoride fiber laser [27]. This result remains the longest wavelength emitted from a fiber laser.

2.3.5 Pulsed Fiber Lasers

Fiber lasers cover a number of pulse width regimes, but the small dimensions of the active core invoke surface damage-threshold limitations. So far, silicate glass fiber has provided the highest peak power, largest pulse energy and widest variety of pulse widths from fiber lasers operating at 2 μm, primarily because of its large damage threshold and the overall maturity of 2 μm fiber lasers. Fiber lasers using Tm^{3+} and Ho^{3+} cations have been mode-locked for ultrashort pulse generation using different approaches [79]-[81]. Because the saturation energy is proportional to the core area, the increased mode size relevant to 2 μm fiber lasers compared with 1 μm fiber lasers benefits energy extraction. Today's shortest pulsewidth at 2 μm from a fiber is 108 fs [82]. Mode-locked fiber lasers operating at 2 μm typically create solitons because silicate fibers are anomalously dispersive at these wavelengths. Larger pulse energies can be achieved by engineering the overall dispersion [83]. Chirped pulse amplification of ultrashort pulses using Tm^{3+}-doped silicate glass fiber leads to near-megawatt peak powers after recompression [84]. For applications that require longer pulses, active Q-switching [85] is capable of generating pulses measuring just a few tens of nanoseconds in duration [86]. Gain-switching [87] using pulsed diode lasers emitting at 1.5 μm for direct excitation of the upper laser level can generate pulses of less than 2 ns in duration [88].

Pulsed fiber laser sources emitting at longer wavelengths make use of fluoride glass, which has a lower surface optical damage threshold but potentially larger mode area than silicate glass. Steady progress has been made with recent demonstrations of Q-switched [89] (90 ns pulsewidth and 0.9 kW peak power) and gain-switched [90] (307 ns pulsewidth and 68 W peak power) operation of Er^{3+}-doped ZBLAN fiber lasers. Recent demonstrations of Q-switched single-transition [91] and cascaded [92] Ho^{3+}-doped fluoride fiber lasers provide 70 ns pulses, emission at 2.87 μm and two-wavelength output. Given that additional mode-size enhancement YF can be achieved by capping the ends of the fiber [41], and that 5 kW peak power has already been demonstrated using fluoride fiber [93], the output performance of pulsed fluoride fiber lasers is likely to see further improvement. The ability to generate clean pulses with smooth transverse mode profiles that prevent localized large intensities will be particularly relevant to future high-peak-power fluoride fiber lasers.

2.4 REFERENCES

[1] Snitzer, E. *et al.* Double clad, offset core Nd fiber laser in *Optical Fiber Sensors*, Vol. 2, Paper PD5 of OSA Technical Digest Series (OSA, 1988).

[2] Zenteno, L. High-power double clad fiber lasers. *J. Lightwave Technol*. 11, 1435-1446 (1993).

[3] Jeong, Y., Sahu, J.K., Payne, D.N. and Nilsson, J. Ytterbium-doped large-core fiber laser with 1.36 kW continuous-wave output power. *Opt. Express* 12, 6088-6092 (2004).

[4] Poole, S.B., Payne, D.N. and Fermann, M.E. Fabrication of low-loss optical fibers containing rare earth ions. *Electron. Lett*. 21, 737-738 (1985).

[5] http://www.ipgphotonics.com/.

[6] Sanghera, J., Shaw, L.B. and Aggarwal, I.D. Chalcogenide glass-fiber-based mid-IR sources and applications, *IEEE J. of Selected Topics in Quantum Electronics* 15, No. 1, 114-119 (2009).

[7] Offerhaus, H.L. *et al.* High-energy single-transverse-mode *Q*-switched fiber laser based on a multimode large-mode-area erbium-doped fiber. *Opt. Lett*. 23, 1683-1685 (1998).

[8] Knight, J.C. *et al.* Large mode area photonic crystal fiber. *Electron. Lett*. 34, 1347-1348 (1998).

[9] Rottwitt, K. *et al.* Scaling of the Raman gain coefficient: applications to germanosilicate fibers. *J. Lightwave Technol*. 21, 1652-1662 (2003).

[10] Koponen, J.J., Söderlund, M.J., Hoffman, H.J. and Tammela, S.K.T. Measuring photodarkening from single-mode ytterbium doped silica fibers. *Opt. Express* 14, 11539-11544 (2006).

[11] Jetschke, S., Unger, S., Röpke, U. and Kirchhof, J. Photodarkening in Yb doped fibers: experimental evidence of equilibrium states depending on the pump power. *Opt. Express* 15, 14838-14843 (2007).

[12] Greaves, G.N. EXAFS and the structure of glass. *J. Non-cryst. Solids* 71, 203-217 (1985).

[13] Caro, P., Beaury, O. and Antic, E. Nephelauxetic effect for 4fN configurations in solid-state. *J. Phys.-Paris* 37, 671-676 (1976).

[14] Jackson, S. Towards high-power mid-infrared emission from a fiber laser. *Nature Photonics* 6, 423-431 (2012).

[15] Jeong, Y. *et al.* Erbium:ytterbium codoped large-core fiber laser with 297 W continuous-wave output power. *IEEE J. Sel. Top. Quant. Electron.* 13, 573-579 (2007).

[16] Eichhorn, M. and Jackson, S.D. Comparative study of continuous wave Tm^{3+}-doped silica and fluoride fiber lasers. *Appl. Phys. B* 90, 35-41 (2008).

[17] Ehrenreich, T. *et al.* 1 kW, all-glass Tm:fiber laser. SPIE Photonics West 2010: LASE, Fibre Lasers VII: Technology, Systems and Applications, Conference 7850 (2010).

[18] Jackson, S.D. *et al.* High-power 83 W holmium-doped silica fiber laser operating with high beam quality. *Opt. Lett.* 32, 241-243 (2007).

[19] Hemming, A. *et al.* A monolithic cladding pumped holmium-doped fiber laser. CLEO: 2013 Technical Digest, Paper CW1M.1, OSA (2013).

[20] El-Agmy, R.M. and Al-Hosiny, N.M. 2.31 μm laser under up-conversion pumping at 1.064 μm in Tm^{3+}:ZBLAN fibre lasers. *Electron. Lett.* 46, 936-937 (2010).

[21] Tokita, S. *et al.* Liquid-cooled 24 W mid-infrared Er:ZBLAN fiber laser. *Opt. Lett.* 34, 3062-3064 (2009).

[22] Jackson, S.D. Single-transverse-mode 2.5-W holmium-doped fluoride fiber laser operating at 2.86 μm. *Opt. Lett.* 29, 334-336 (2004).

[23] Jackson, S.D. Continuous wave 2.9 μm dysprosium-doped fluoride fiber laser. *Appl. Phys. Lett.* 83, 1316-1318 (2003).

[24] Li, J., Hudson, D.D. and Jackson S.D. High-power diode-pumped fiber laser operating at 3 μm. *Opt. Lett.* 36, 3642-3644 (2011).

[25] Carbonnier, C., Többen, H. and Unrau, U.B. Room temperature CW fibre laser at 3.22 μm. *Electron. Lett.* 34, 893-894 (1998).

[26] Tobben, H. Room temperature CW fibre laser at 3.5 μm in Er3+-doped ZBLAN glass. *Electron. Lett.* 28, 1361-1363 (1992).

[27] Schneider, J., Carbonnier, C. and Unrau, U.B. Characterization of a Ho3+-doped fluoride fiber laser with a 3.9 μm emission wavelength. *Appl. Opt.* 36, 8595-8600 (1997).

[28] Brown, D.C. and Hoffman, H.J. Thermal, stress, and thermo-optic effects in high average power double-clad silica fiber lasers. *IEEE J. Quant. Electron*. 37, 207-217 (2001).

[29] Esterowitz, L., Eckardt, R.C. and Allen, R.E. Long-wavelength stimulated-emission via cascade laser action in Ho-YLF. *Appl. Phys. Lett*. 35, 23-239 (1979).

[30] Hanna, D.C., Percival, R.M., Smart, R.G. and Tropper, A.C. Efficient and tunable operation of a Tm-doped fibre laser. *Opt. Commun.* 75, 283-286 (1990).

[31] Jackson, S.D. and King, T.A. High-power diode-cladding-pumped Tm-doped silica fiber laser. *Opt. Lett*. 23, 1462-1464 (1998).

[32] Hayward, R.A. *et al.* Efficient cladding-pumped Tm-doped silica fibre laser with high power single-mode output at 2 μm. *Electron. Lett*. 36, 711-712 (2000).

[33] Moulton, P.F. *et al.* Tm-doped fiber lasers: fundamentals and power scaling. *IEEE J. Sel. Top. Quant. Electron.* 15, 85-92 (2009).

[34] Clarkson, W.A. *et al.* High-power cladding-pumped Tm-doped silica fiber laser with wavelength tuning from 1860 to 2090 nm. *Opt. Lett*. 27, 1989-1991 (2002).

[35] Jackson, S.D. Cross relaxation and energy transfer upconversion processes relevant to the functioning of 2 μm Tm3+-doped silica fibre lasers. *Opt. Commun.* 230, 197-203 (2004).

[36] Jackson, S.D. Midinfrared holmium fiber lasers. *IEEE J. Quant. Electron*. 42, 187-191 (2006).

[37] Oh, K. *et al.* Continuous-wave oscillation of thulium-sensitized holmium-doped silica fiber laser. *Opt. Lett.* 19, 278-280 (1994).

[38] Jackson, S.D., Bugge, F. and Erbert, G. Directly diode-pumped holmium fiber lasers. *Opt. Lett.* 32, 2496-2498 (2007).

[39] Tokita, S. *et al.* Stable 10 W Er:ZBLAN fiber laser operating at 2.71–2.88 μm. *Opt. Lett.* 35, 3943-3945 (2010).

[40] Faucher, D. *et al.* 20 W passively cooled single-mode all-fiber laser at 2.8 μm. *Opt. Lett.* 36, 1104-1106 (2011).

[41] Bernier, M. *et al.* Bragg gratings photoinduced in ZBLAN fibers by femtosecond pulses at 800 nm. *Opt. Lett.* 32, 454-456 (2007).

[42] Faucher, D., Bernier, M., Caron, N. and Vallee, R. Erbium-doped all-fiber laser at 2.94 μm. *Opt. Lett.* 34, 3313-3315 (2009).

[43] Gorjan, M., Marincek, M. and Copic, M. Role of interionic processes in the efficiency and operation of erbium-doped fluoride fiber lasers. *IEEE J. Quant. Electron*. 47, 262-273 (2011).

[44] Schneider, J. Mid-infrared fluoride fiber lasers in multiple cascade operation. *IEEE Photon. Tech. Lett.* 7, 354-356 (1995).

[45] Pollnau, M. *et al.* Three-transition cascade erbium laser at 1.7, 2.7, and 1.6 μm. *Opt. Lett.* 22, 612-614 (1997).

[46] Jackson, S.D. High-power erbium cascade fibre laser. *Electron. Lett*. 45, 830-832 (2009).

[47] Li, J. and Jackson, S.D. Numerical modeling and optimization of diode pumped heavily-erbium-doped fluoride fiber lasers. *IEEE J. Quant. Electron*. 48, 454-464 (2012).

[48] Wetenkamp, L., West, G.F. and Tobben. H. Optical properties of rare earth-doped ZBLAN glasses. *J. Non-cryst. Solids* 140, 35-40 (1992).

[49] Hruby, A. Evaluation of glass-forming tendency by means of DTA. *Czech J. Phys*. B22, 1187-1193 (1972).

[50] Tünnermann, A. *et al.* The renaissance and bright future of fibre lasers. *J. Phys. B* 38, S681-S693 (2005).

[51] Layne, C.B., Lowdermilk, W.H. and Weber, M.J. Multiphonon relaxation of rare-earth ions in oxide glasses. *Phys. Rev. B* 16, 10-20 (1977).

[52] Saito, K. *et al.* Limit of the Rayleigh scattering loss in silica fiber. *Appl. Phys. Lett*. 83, 5175-5177 (2003).

[53] Arai, K. *et al.* Aluminium or phosphorous co-doping effects on the fluorescence properties of neodymium-doped silica glass. *J. Appl. Phys*. 59, 3430-3436 (1986).

[54] Sacks, Z.S., Schiffer, Z. and David, D. Long wavelength operation of double-clad Tm:silica fiber lasers. *Proc. SPIE* 6453, 645320 (2007).

[55] Ohsawa, K., Shibata, T., Nakamura, K. and Yoshida, S. Fluorozirconate glasses for infrared transmitting optical fibers. Paper 1.1, Technical Digest, 7th European Conference on Optical Communication (1981).

[56] Mitachi, S., Miyashita, T. and Kanamori, T. Fluoride-glass cladded optical fibers for mid-infra-red ray transmission. *Electron. Lett*. 17, 591-592 (1981).

[57] Tran, D.C., Fisher, C.F. and Sigel, G.H. Jr. Fluoride glass performs prepared by a rotation casting process. *Electron. Lett*. 18, 657-658 (1982).

[58] Carter, S.F. *et al.* Low loss fluoride fibre by reduced pressure casting. *Electron. Lett*. 26, 2115-2117 (1990).

[59] Almeida, R.M. and Mackenzie, J.D. Vibrational spectra and structure of fluorozirconate glasses. *J. Chem. Phys*. 74, 5954-5961 (1981).

[60] Day, C.R. *et al.* Fluoride fibres for optical transmission. *Opt. Quant. Electron*. 22, 259-277 (1990).

[61] Zhu, X. and Jain, R. 10-W-level diode-pumped compact 2.78 μm ZBLAN fiber laser. *Opt. Lett*. 32, 26-28 (2007).

[62] Fortin, V., Bernier, M., Carrier, J. and Vallée, R. Fluoride glass Raman fiber laser at 2185 nm. *Opt. Lett*. 36, 4152-4154 (2011).

[63] Wang, J., *et al.* Fabrication and optical-properties of lead-germanate glasses and a new class of optical fiber lasers doped with Tm3+, *J. Appl. Phys.* 73, 8066-8075 (1993).

[64] Lincoln, J.R. *et al.* New class of fibre laser based on lead-germanate glass. *Electron. Lett.* 28, 1021-1022 (1992).

[65] Wu, J., Yao, Z., Zong, J. and Jiang, S. Highly efficient high-power thulium-doped germanate glass fiber laser. *Opt. Lett*. 32, 638-640 (2007).

[66] Geng, J., Wu, J., Jiang, S. and Yu, J. Efficient operation of diode-pumped single-frequency thulium-doped fiber lasers near 2 μm. *Opt. Lett*. 32, 355-357 (2007).

[67] Mori, A., Ohishi, Y. and Sudo, S. Erbium-doped tellurite glass fibre laser and amplifier. *Electron. Lett*. 33, 863-864 (1997).

[68] Gomes, L. *et al.* Energy level decay and excited state absorption processes in erbium-doped tellurite glass. *J. Appl. Phys*. 110, 083111 (2011).

[69] Eggleton, B.J., Luther-Davies, B. and Richardson, K. Chalcogenide photonics. *Nature Photon.* 5, 141-148 (2011).

[70] Julien, C. *et al.* Raman and infrared spectroscopic studies of Ge–Ga–Ag sulfide glasses. *Mat. Sci. Eng*. B22, 191-200 (1994).

[71] Weszka, J. *et al.* Raman scattering in In2Se3 and InSe2 amorphous films. *J. Non-cryst. Solids* 265, 98-104 (2000).

[72] Uemura, O., Hayasaka, N., Tokairin, S. and Usuki, T. Local atomic arrangement in Ge–Te and Ge–S–Te glasses. *J. Non-cryst. Solids* 205, 189-193 (1996).

[73] Maurugeon, S. *et al.* Telluride glass step index fiber for the far infrared. *J. Lightwave Technol*. 28, 3358-3363 (2010).

[74] Shaw, L.B., Cole, B., Thielen, P., Sanghera, J. and Aggarwal, I.D. Mid-wave IR and long-wave IR laser potential of rare earth doped chalcogenide glass fiber. *IEEE J. Quantum Electronics* 37 1127-1137 (2001).

[75] Schweizer, T. *et al.* Rare-earth doped chalcogenide glass laser. *Electron. Lett*. 32, 666-667 (1996).

[76] Brady, D.J. and Schweizer, T. Minimum loss predictions and measurements in gallium lanthanum sulfide based glasses and fibers. *J. Non-cryst. Solids* 242, 92-98 (1998).

[77] Seddon, A.B. *et al.* Progress in rare-earth-doped mid-infrared fiber lasers. *Opt. Express* 18, 26704-26719 (2010).

[78] Aggarwal, I.D. and Sanghera, J.S. Development and applications of chalcogenide glass optical fibers at NRL. *J. Optoelectron. Adv. Mat*. 4, 665-678 (2002).

[79] Nelson, L.E., Ippen, E.P. and Haus, H.A. Broadly tunable sub-500 fs pulses from an additive-pulse mode-locked thulium-doped fiber ring laser. *Appl. Phys. Lett*. 67, 19-21 (1995).

[80] Sharp, R.C., Spock, D.E., Pan, N. and Elliot, J. 190-fs passively mode-locked thulium fiber laser with a low threshold. *Opt. Lett*. 21, 881-883 (1996).

[81] Solodyankn, M.A. *et al.* Mode-locked 1.93 μm thulium laser with a carbon nanotube absorber. *Opt. Lett*. 33, 1336-1338 (2008).

[82] Imeshev, I. and Fermann, M.E. 230-kW peak power femtosecond pulses from a high power tunable source based on amplification in Tm-doped fiber. *Opt. Express* 13, 7424-7431 (2005).

[83] Engelbrecht, M., Haxsen, F., Ruehl, A., Wandt, D. and Kracht, D. Ultrafast thulium-doped fiber-oscillator with pulse energy of 4.3 nJ. *Opt. Lett*. 33, 690-692 (2008).

[84] Haxsen, F. *et al.* Pulse energy of 151-nJ from ultrafast thulium-doped chirped-pulse fiber amplifier. *Opt. Lett*. 35, 2991-2993 (2010).

[85] El-Sherif, A.F. and King, T.A. High-peak-power operation of a *Q*-switched Tm^{3+}-doped silica fiber laser operating near 2 μm. *Opt. Lett*. 28, 22-24 (2003).

[86] Eichhorn, M. and Jackson, S.D. High-pulse-energy actively *Q*-switched Tm^{3+}-doped silica 2 μm fiber laser pumped at 792 nm. *Opt. Lett*. 32, 2780-2782 (2007).

[87] Jiang, M. and Tayebati, P. Stable 10 ns, kilowatt peak-power pulse generation from a gain-switched Tm-doped fiber laser. *Opt. Lett*. 32, 1797-1799 (2007).

[88] Ding, J.W. *et al.* A monolithic thulium doped single mode fiber laser with 1.5 ns pulsewidth and 8 kW peak power. *Proc. SPIE* 7914, 79140X (2011).

[89] Tokita, S. *et al.* 12 W *Q*-switched Er:ZBLAN fiber laser at 2.8 μm. *Opt. Lett*. 36, 2812-2814 (2011).

[90] Gorjan, M., Petkovšek, R., Marinček, M. and Čopič, M. High-power pulsed diode-pumped Er:ZBLAN fiber laser. *Opt. Lett*. 36, 1923-1925 (2011).

[91] Hu, T., Hudson, D.D. and Jackson, S.D. Actively *Q*-switched 2.9 μm $Ho^{3+}Pr^{3}$+-doped fluoride fiber laser. *Opt. Lett*. 37, 2145-2147 (2012).

[92] Li, J., Hu, T. and Jackson, S.D. *Q*-switched fiber cascade laser. *Opt. Lett*. 37, 2208-2210 (2012).

[93] Eichhorn, M. High-peak-power Tm-doped double-clad fluoride fiber amplifier. *Opt. Lett*. 30, 3329-3331 (2005).